RSC Advances

Journal Name

RSC Advances

ARTICLE TYPE

Flexible Ribbon-shaped Coaxial Electrical Conductive Nanocables Array Endowed with Magnetism and Photoluminescence

Qianli Ma, Jinxian Wang, Xiangting Dong,* Wensheng Yu and Guixia Liu

A new type of flexible [Fe$_3$O$_4$/polyaniline (PANI)/PMMA]@[Tb(BA)$_3$phen/PMMA] ribbon-shaped coaxial conductive nanocables array possessing conductivity, magnetism and photoluminescence has been successfully fabricated by electrospinning technology using a specially designed coaxial spinneret. Every single ribbon-shaped coaxial nanocable in the array is assembled with a Fe$_3$O$_4$/PANI/PMMA electric conductive-magnetic bifunctional core with tunable width and a Tb(BA)$_3$phen/PMMA insulating photoluminescent sheath. All the ribbon-shaped coaxial nanocables are insulated with each other and arranged in array alignment. The conductivity of the core of each ribbon-shaped coaxial nanocable reaches up to the order of 10^{-2} S·cm^{-1}, and the electric conductance of each single ribbon-shaped coaxial conductive nanocable can be calculated by formula and available experimental data. The ribbon-shaped coaxial nanocables array is simultaneously endowed with magnetic and photoluminescent characteristics for improving controllability and visibility. The electrical conductivity, magnetic and photoluminescent properties of ribbon-shaped coaxial nanocables array can be tunable by adjusting the contents of PANI and Fe$_3$O$_4$ nanoparticles and rare earth complexes, or by varying the width of the cores of the every ribbon-shaped coaxial nanocable in the array. This nanostructure is ideally suited to be applied in high density electrical connection in narrow space, such as in mobile phones, subminiature integrated circuits, microchips and nano-machines.

Introduction

Ribbon-shaped one-dimensional (1D) materials have attracted increasing interest from scientists owing to their anisotropy, large width-thickness ratio, and unique optical, electrical, and magnetic properties. More and more manufacturers use ribbon-shaped cables as conductive lines because the ribbon-shaped cables have better anti-entangling performance and smaller winding volume than the traditional cables in round section (See **Figure 1a** and **b**). Multi-wire planar cable is a cable with many conducting wires running parallel to each other on the same flat plane. Multi-wire planar cables are usually seen for internal peripherals in computers, such as hard drives, CD drives and floppy drives (See **Figure 1c** and **d**).
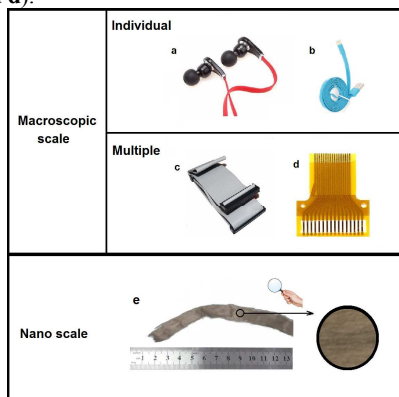
Fig. 1 Practical applications of macro-sized ribbon-shaped cables: headphone cable (a), data cable for mobile phone (b), parallel ATA cable (c) and flexible flat cable (FFC) (d), and a digital photo of flexible [Fe$_3$O$_4$/PANI/PMMA]@[Tb(BA)$_3$phen/PMMA] ribbon-shaped coaxial conductive nanocables array (e)

With the rapid development of nanotechnology in recent years, fabrication and application of electroconductive nanowires

and nanocables are becoming more and more crucial. Up to now, some types of nanocables have been synthesized. The researchers have adoped carbon fibers or tubes, metal materials, conductive polymers and other conductive materials as the inner conductor of nanocables.[1-6] The sheath must have good insulation property and, sometimes, have other functions. Many methods are used for the fabrication of nanocables, including hydrothermal, template, deposition and electrospinning method, etc. Guo et al. synthesized well-defined silica-coated carbon nanotube coaxial nanocable via the combination of sonication and sol-gel techniques.[7] Zhou et al. investigated the properties of BN nanotubes filled with close-packed Cu nanowires by gradient-corrected density functional theory computations.[8] Song et al. fabricated core-sheath silver nanowire/polyvinylpyrrolidone nanocables via an efficient single-spinneret electrospinning method.[9] Jang et al. fabricated polypyrrole/poly(methyl methacrylate) coaxial nanocable through the sequential polymerization of methyl methacrylate and pyrrole monomers inside the channels of mesoporous SBA-15 silica, followed by the removal of the silica template.[10] Based on the characterizations of the products described in references, it is found that the most of the reported conductive nanocables have some deficiencies. Firstly, some kinds of nanocables are quite brittle, resulting in the poor deformation, bending and stretch ability; secondly, the lengths of most types of the products are very small (even less than 1 cm) due to the limitation of preparation methods; thirdly, in order to obtain the nanocables with core-sheath structure, two steps are usually needed by most of the preparation methods, leading to the long production period and high cost. Fourthly, the nanocables are hard to install to the instruments, because it is hard to observe them due to their too small diameters. All of these deficiencies restrict the practical applications of conductive nanocables.

Electrospinning technique has been widely adoped to

effectively fabricate 1D nanomaterials, and has been applied in many areas such as filtration,[11] optical and chemical sensors,[12] biological scaffolds,[13] electrode materials,[14] luminescent materials,[15] photocatalysts.[16,17] The electrospun products have some unique advantages, such as long length (up to several meters), good flexibility (owing to the polymer template) and low-power consumption. The order of the electrospun products can also be arranged by controlling the collector.[18-20] In recent years, our research group has made some progress in the electrospun flexible 1D magnetic-photoluminescent bifunctional nanomaterials.[21-24] The obtained 1D magnetic-photoluminescent bifunctional nanomaterials simultaneously possess controllability (by magnetic field) and visibility (by emitting visible light).

Inspired by the unique properties of the flexible 1D magnetic-photoluminescent bifunctional nanomaterials, the controllability, visibility, flexibility and length of the nanocables can be improved once endowing the nanocables magnetic and photoluminescent properties and fabricating via electrospinning technique. Thus, in this work, novel ribbon-shaped flexible coaxial conductive nanocables with magnetic and photoluminescent properties were fabricated via electrospinning technique, and a new kind of coaxial spinneret was designed and manufactured to fabricate the ribbon-shaped coaxial nanocables. The tunable core of the ribbon-shaped coaxial nanocables is composed of conductive polyaniline (PANI), magnetic Fe_3O_4 nanoparticles (NPs) and PMMA template; the sheath consists of photoluminescent $Tb(BA)_3$phen complexes and PMMA template. In order to enhance the conductivity of PANI in the core, the aniline (ANI) was polymerized in the mixture solution of PMMA, DMF and CH_3Cl. Furthermore, the ribbon-shaped coaxial conductive nanocables were arranged in array alignment by using a rolling aluminum rotary drum as the collector. The ribbon-shaped coaxial nanocables, as well as their arrays, were firstly fabricated in this study. Furthermore, it is the first time that the electric conductive nanocables were endowed with magnetic and photoluminescent properties. The structure, conductivity, fluorescence, and magnetism of the ribbon-shaped coaxial conductive nanocables arrays were studied, and some new results were obtained. The obtained ribbon-shaped coaxial conductive nanocables arrays take over many deficiencies of the existing conductive nanocables as mentioned above. The synthesized multifunctional ribbon-shaped coaxial conductive nanocables arrays will have important potential application perspective in high-density interconnection. Furthermore, the design concept and preparation method of the ribbon-shaped coaxial nanocables arrays are of universal significance for the fabrication of other types of ribbon-shaped coaxial nanocables arrays.

Experimental Sections

Chemicals

Methylmethacrylate (MMA), benzoylperoxide (BPO), Tb_4O_7, benzoic acid (BA), 1,10-phenanthroline (phen), $FeCl_3 \cdot 6H_2O$, $FeSO_4 \cdot 7H_2O$, NH_4NO_3, polyethylene glycol (PEG, Mr≈20000), ammonia, oleic acid (OA), aniline (ANI), (IS)-(+)-camphor-10 sulfonic acid (CSA), ammonium persulfate (APS), anhydrous ethanol, $CHCl_3$, N,N-dimethylformamide (DMF), and deionized water were used. All the reagents were of analytical grade. The purity of Tb_4O_7 was 99.99 %. The deionized water was homemade.

Preparation of OA modified Fe_3O_4 NPs

Fe_3O_4 NPs with the saturation magnetization of 62.02 emu·g^{-1} were obtained by using a facile coprecipitation synthetic method.[25] To improve the monodispersity, stability, and solubility of Fe_3O_4 NPs in the spinning solution, the as-prepared Fe_3O_4 NPs were coated with OA as below: 1.5 g of the as-prepared Fe_3O_4 NPs were ultrasonically dispersed in 50 mL of deionized water for 20 min. The suspension was heated to 80 °C under an argon atmosphere with vigorous mechanical stirring for 30 min and then 0.5 mL of OA was slowly added. The reaction was stopped after heating and stirring the mixture for 40 min. The precipitates were collected from the solution by magnetic separation, washed with ethyl alcohol for three times, and then dried in an electric vacuum oven at 60 °C for 6 h. Then, all of the products were used to prepare the core spinning solution.

Synthesis of $Tb(BA)_3$phen complexes

$Tb(BA)_3$phen powders were synthesized according to the traditional method as described in the literature.[26]

Preparation of PMMA

PMMA used in this study was prepared by oxidative polymerization of MMA. The detailed synthetic process was provided in the reference.[23]

Preparation of spinning solutions for fabricating magnetic-photoluminescent ribbon-shaped coaxial conductive nanocables array

Two different kinds of spinning solutions were prepared to fabricate the coaxial nanocables array. The spinning solution for the core of coaxial nanocables array was composed of CSA doped PANI, OA modified Fe_3O_4 NPs, PMMA, $CHCl_3$, and DMF (core spinning solution). In the preparation of core spinning solutions, 0.5000 g of PMMA was dissolved into the mixed solution of 9.3750 g of $CHCl_3$ and 0.6250 g of DMF under magnetic stirring for 48 h. The mixture was then cooled down to 0 °C in an ice-bath. In order to find the optimum adding dosage of ANI, various amounts of ANI and CSA were added into the above mixture and kept stirring for 2 h, followed by introducing of APS and stirring for 30 min. The final mixture was allowed to react at 0 °C for 24 h and then the as-prepared OA modified Fe_3O_4 NPs were added into the mixture under mechanical stirring for 2 h at room temperature, thus the core spinning solution was prepared. For performing the electrical conductivity tests, 2 mL of the core spinning solution was dripped onto a piece of glass and the solvent was allowed to completely volatilize at room temperature for 48 h. The dosages of ANI, CSA, APS and the corresponding conductivities were shown in **Table 1**. One can see that the conductivity reaches up to the order of 10^{-2} S·cm^{-1}, and it increases not much with adding more ANI than 0.1500 g. Thus the core spinning solution containing 0.1500g ANI was adopted for the following study.

Table 1 Dosages of ANI, CSA, APS and corresponding conductivities

ANI (g)	CSA (g)	APS (g)	Conductivity (S·cm^{-1})
0.0500	0.0625	0.1225	1.974×10^{-6}
0.1000	0.1249	0.2450	3.931×10^{-4}
0.1500	0.1873	0.3676	1.092×10^{-2}
0.2000	0.2497	0.4900	1.475×10^{-2}
0.2500	0.3125	0.6125	1.874×10^{-2}

Another spinning solution for the sheath of the coaxial nanocables array consisted of $Tb(BA)_3$phen, PMMA, $CHCl_3$, and DMF (sheath spinning solution). It has been known through our previous work that the optimum ratio of $Tb(BA)_3$phen to PMMA is 1:10. [27] Thus for the preparation of the sheath spinning solutions, 0.5000 g of PMMA and 0.0500 g of $Tb(BA)_3$phen were added into the mixed solution of 9.3750 g of $CHCl_3$ and 0.6250 g

of DMF under magnetic stirring for 48 h.

Electrospinning equipment for fabricating magnetic-photoluminescent ribbon-shaped coaxial conductive nanocables array

Coaxial electrospinning technology has recently matured for fabricating coaxial nanofibers and hollow nanofibers.[28,29] Nearly all types of spinnerets for coaxial electrospinning are composed of two stainless-steel needles of different diameters using one inside the other. We found the traditional coaxial spinnerets have some disadvantages when we attempted to use them to fabricate coaxial nanoribbons in our previous work, and a modified coaxial spinneret was designed and manufactured to fabricate coaxial nanoribbons.[27] The assembly diagram of the modified coaxial spinneret is shown in **Figure S1** in Supporting Information. As illustrated in **Figure S1**, two kinds of spinning solution had formed a coaxial structure before they flowed to the tip of the plastic nozzle, and the Taylor cone remained in this coaxial structure. This illustrates how the structure of the final products reflected the structure of the spinning solutions approaching the tip of the spinneret and the Taylor cone. We have successfully fabricated coaxial nanoribbons via electrospinning using the modified coaxial spinneret.

Another advantage of the modified coaxial spinneret was that the width of the core of the fabricated ribbon-shaped coaxial nanocables could be tunable easily only by changing the diameter of the inner stainless-steel needle without readjusting other spinning parameters. In this work, the ribbon-shaped coaxial nanocables with three different widths of their cores were fabricated using inner stainless-steel needles with three different diameters, including 7 # (inner/outer diameter: 0.41/0.71 mm), 12 # (0.90/1.26 mm) and 16 # (1.25/1.61 mm). Unless otherwise indicated, the products were fabricate using 16 # inner stainless-steel needle in the following text. To our knowledge, this is the first report that the width of the core of an electrospun 1D coaxial nanomaterial can be tuned just by changing the inner stainless-steel needle.

The equipment for the electrospinning process is presented in **Figure 2**. The core spinning solution was injected into the inner plastic syringe while the sheath spinning solution was loaded into the outer one. In order to obtain nanocables array, an aluminum rotary drum was used as a nanocables collector, which was put about 18 cm away from the tip of the plastic nozzle. The aluminum rotary drum was 20 cm in length, 7 cm in diameter, fixed in horizontal, and the rotation speed was 1500 r·min^{-1}. A positive direct current (DC) voltage of 6 kV was applied between the spinneret and the collector to generate stable, continuous PMMA-based nanocables array at 20-22 °C and the relative humidity of 20-30 %. In the electrospinning process, the two spinning solutions at the tip of the plastic nozzle have formed a coaxial structure, and they are then stretched by electric field force to form a coaxial Taylor cone and a coaxial jet. The coaxial jet is stretched to ribbon shape by electrostatic repulsion and solidified with the volatilization of solvents, thus ribbon-shaped coaxial nanocable is obtained. A more detailed formation mechanism of electrospun ribbon-shaped coaxial nanocable is proposed in Supporting Information. Furthermore, because the coaxial nanocable swings in the air due to the instability of electrospinning process, an array with a certain width can be collected on the surface of the aluminum rotary drum.
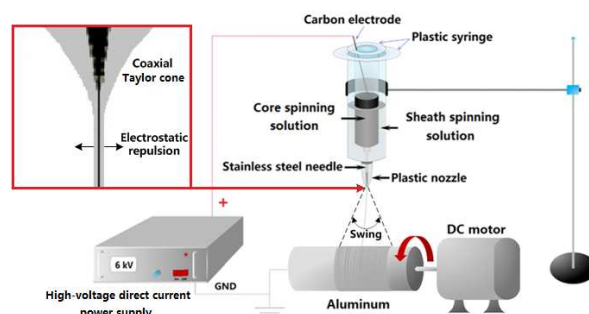
Fig. 2 Schematic diagram of the equipment for the electrospinning process of ribbon-shaped coaxial conductive nanocables array

Characterization

The phase compositions were identified by an X-ray powder diffractometer (Bruker, D8 FOCUS) with CuKα radiation. The operation voltage and current were kept at 40 kV and 20 mA, respectively. The morphologies and internal structures were observed by a field-emission scanning electron microscope (FESEM, XL-30) and a biological microscope (CVM500E), respectively. The elemental analysis was performed by an energy-dispersive spectrometer (Oxford Instruments) attached to the FESEM. The conductivity properties were measured by a Hall effect measurement system (ECOPIA HMS-3000) using Van der Pauw method. The fluorescent properties were investigated by Hitachi fluorescence spectrophotometer F-7000. The UV-vis absorption spectra were tested by a UV-Vis spectrophotometer (SHIMADZU UV mini 1240). Then, the magnetic performances were measured by a vibrating sample magnetometer (VSM, MPMS SQUID XL).

Results and Discussion

Phase analyses

The phase compositions of the Fe_3O_4 NPs and $[Fe_3O_4/PANI/PMMA]@[Tb(BA)_3phen/PMMA]$ ribbon-shaped coaxial conductive nanocables array were characterized by means of X-ray diffractometry (XRD) analysis, as shown in **Figure 3**. The XRD patterns of the as-prepared Fe_3O_4 NPs conform to the cubic structure of Fe_3O_4 (PDF 74-0748), and no characteristic peaks are observed for other impurities such as Fe_2O_3 and FeO(OH). The XRD analysis results of the nanocables array demonstrate that the nanocables array contain Fe_3O_4 NPs, and the broad diffraction peak at 15 ° can be attributed to the amorphous PMMA, PANI and $Tb(BA)_3phen$.
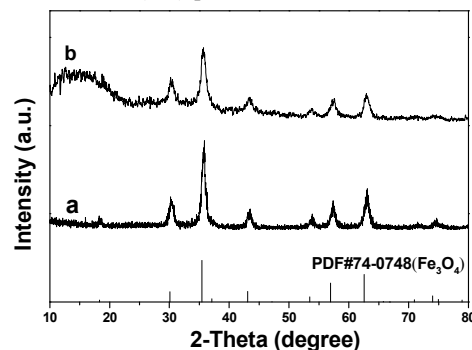
Fig. 3 XRD patterns of the Fe_3O_4 NPs (a) and $[Fe_3O_4/PANI/PMMA]@[Tb(BA)_3phen/PMMA]$ ribbon-shaped coaxial conductive nanocables array (b)

Morphology and internal structure

The morphology of the as-prepared Fe_3O_4 NPs was observed by means of SEM, as presented in **Figure 4a**. The size distribution of the spherical Fe_3O_4 NPs is almost uniform, and the particle size of the NPs is 9.06±0.79 nm (**Figure 4b**). The macro-appearance of the $[Fe_3O_4/PANI/PMMA]@[Tb(BA)_3phen/PMMA]$ ribbon-shaped coaxial conductive nanocables array is shown in **Figure 1e**. The ribbon-shaped coaxial conductive nanocables array is flexible, and its length is greater than 10 cm. The SEM image of the $[Fe_3O_4/PANI/PMMA]@[Tb(BA)_3phen/PMMA]$ ribbon-shaped coaxial conductive nanocables array was shown in **Figure 4c**. The width of every single ribbon-shaped coaxial conductive nanocable is ca. 10 μm and the thickness is about 879 nm. All the ribbon-shaped coaxial conductive nanocables are arranged in the same direction. Depending on the transmission light of the BM, the inner structures of the ribbon-shaped coaxial conductive nanocables can be observed. As revealed in **Figure 4d**, a clear coaxial structure can be seen in the ribbon-shaped coaxial conductive nanocables. The cores of them contain large quantities of dark-colored PANI and Fe_3O_4 NPs, and the sheaths are transparent.
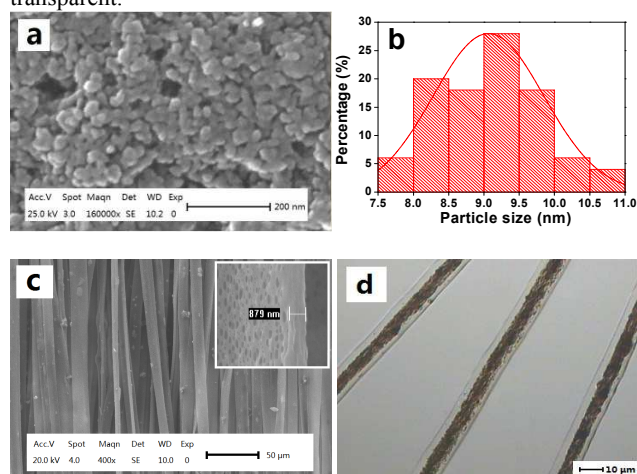
Fig. 4 SEM image (a) and histogram of particle size (b) of Fe_3O_4 NPs; SEM image (c) and BM image (d) of $[Fe_3O_4/PANI/PMMA]@[Tb(BA)_3phen/PMMA]$ ribbon-shaped coaxial conductive nanocables array

In order to further demonstrate the coaxial structure of the a ribbon-shaped coaxial conductive nanocable in the array, EDS line-scan analysis was performed, in which S, Fe and Tb elements represent PANI, Fe_3O_4 and $Tb(BA)_3phen$, respectively, as shown in **Figure 5**. Elemental S and Fe only exist in the middle domain of the ribbon-shaped coaxial conductive nanocable. The amount of elemental Tb in the middle domain of the ribbon-shaped coaxial conductive nanocable is lower than that in both sides of the ribbon-shaped coaxial conductive nanocable because Tb only exists in the top and bottom surfaces of the middle domain of the ribbon-shaped coaxial conductive nanocable. It is further found that only elemental Tb without elemental S and Fe is dispersed in both sides of the ribbon-shaped coaxial conductive nanocable. These results are consistent with the core-sheath structure.
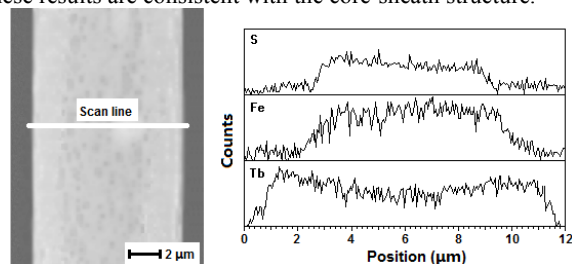
Fig. 5 EDS line-scan analysis of a single

$[Fe_3O_4/PANI/PMMA]@[Tb(BA)_3phen/PMMA]$ ribbon-shaped coaxial conductive nanocable in array

The BM images of the ribbon-shaped coaxial conductive nanocables respectivly fabricated using 7 #, 12 # and 16 # inner stainless-steel needles are revealed in **Figure 6**. It can be seen that the width of the core is increased with the increase of the diameter of the inner stainless-steel needle, demonstrating that the width of the core of the fabricated ribbon-shaped coaxial nanocables can be tunable easily only by changing inner stainless-steel needles without readjusting other spinning parameters.

From the SEM and BM observations, and the EDS line-scan analysis, we have clearly proven that the $[Fe_3O_4/PANI/PMMA]@[Tb(BA)_3phen/PMMA]$ ribbon-shaped coaxial conductive nanocables array with a new and interesting nanostructure has been successfully fabricated.
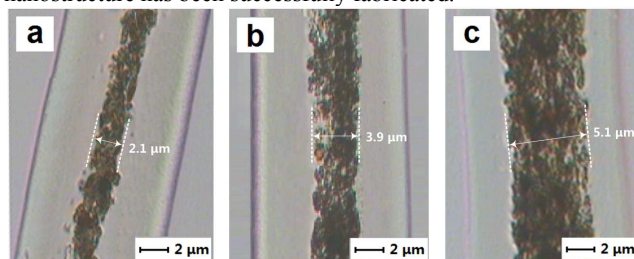
Fig. 6 BM images of ribbon-shaped coaxial conductive nanocables respectivly fabricated using 7 # (a), 12 # (b) and 16 # (c) inner stainless-steel needles

Electrical conductivity analyses

Figure S4 shows the schematic diagram of electrical property of ribbon-shaped coaxial conductive nanocables array. Generally, a conductor and an insulator respectively refer to the materials with the conductivity range of $> 10^{-3}$ S·cm^{-1} and $< 10^{-9}$ S·cm^{-1}, and a semiconductor is a material whose electrical conductivity is intermediate between that of a conductor and an insulator. As described in the previous section, the conductivity of the cores we used in the $[Fe_3O_4/PANI/PMMA]@[Tb(BA)_3phen/PMMA]$ ribbon-shaped coaxial conductive nanocables in the array is 1.092×10^{-2} S·cm^{-1}. In order to investigate the insulativity of each ribbon-shaped coaxial conductive nanocable with each other in the array, the surface conductivities of the arrays, including fabricated using 7 #, 12 # and 16 # inner stainless-steel needles, were also measured by Van der Pauw method. The results (**Table 2**) reveal that the surface conductivity of all the arrays are lower than the order of 10^{-10} S·cm^{-1}, indicating that every ribbon-shaped coaxial conductive nanocable in array is well insulated with each other.

Table 2 The surface conductivities of ribbon-shaped coaxial conductive nanocables arrays fabricated using 7 # (a), 12 # (b) and 16 # (c) inner stainless-steel needles

Sample	Conductivity (S·cm^{-1})
a	4.151×10^{-11}
b	6.274×10^{-11}
c	6.581×10^{-11}

The electric conductance of the core of each single ribbon-shaped coaxial conductive nanocable can be calculated by the formula $G=\kappa(A/l)$, in which G, κ, A and l respectively represent electric conductance, electric conductivity, cross-sectional area and length. The value of κ can be obtained by testing the dried core spinning solution, as indicated in Experimental Section. The value of A can be calculated by the formula $A=T_s\times W_c^2/W_s$, in which T_s, W_s and W_c respectively represent the thickness of the single ribbon-shaped coaxial nanocable, the width of the single ribbon-shaped coaxial nanocable and width of the core of the

ribbon-shaped coaxial nanocable (The deriving process of this formula is provided in Supporting Information), and these parameters can be obtained through SEM and BM observation. After determination of these parameters, the value of electric conductance of each single ribbon-shaped coaxial conductive nanocable with a given length can be obtained by calculation. Furthermore, the κ can be tuned by adding different amount of ANI, CSA and APS into the core spinning solution, as well as the A can be tuned through changing the width of the core by using different inner stainless-steel needles, so that the electric conductance of each single ribbon-shaped coaxial conductive nanocable with a given length is tunable.

Photoluminescence properties

The sheath of a single coaxial conductive nanocable not only can keep insulating from other nanocables, but also provides photoluminescence property in order to improve the visibility of the ribbon-shaped coaxial conductive nanocables array. As seen in the **Figure 7**, the ribbon-shaped coaxial conductive nanocables array can emit green light under the excitation of 333-nm ultraviolet light.
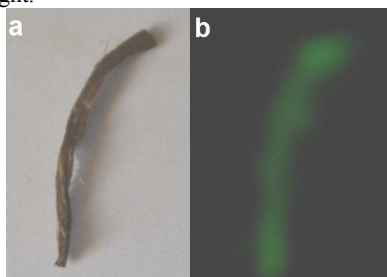
Fig. 7 Digital photos of $[Fe_3O_4/PANI/PMMA]@[Tb(BA)_3phen/PMMA]$ ribbon-shaped coaxial conductive nanocables array taken in natural light (a) and under the excitation of 333-nm ultraviolet light in the darkness (b)

It has been proven in our previous work that the optimum exciting ultraviolet light for $Tb(BA)_3phen/PMMA$ composite materials is at 333 nm,[26] thus the 333-nm ultraviolet light was used to excite the $[Fe_3O_4/PANI/PMMA]@[Tb(BA)_3phen/PMMA]$ ribbon-shaped coaxial conductive nanocables arrays in this work. The left figure in **Figure 8** shows the photoluminescence emission spectra of the ribbon-shaped coaxial conductive nanocables arrays fabricated using different inner stainless-steel needles. Characteristic emission peaks of Tb^{3+} are observed in these products under the excitation of 333-nm ultraviolet light and ascribed to the energy levels transitions of $^5D_4 \rightarrow ^5F_6$ (495 nm), $^5D_4 \rightarrow ^5F_5$ (544 nm), $^7D_4 \rightarrow ^5F_4$ (588 nm), and $^5D_4 \rightarrow ^7F_3$ (624 nm), and the $^5D_4 \rightarrow ^5F_5$ hypersensitive transition at 544 nm is the

predominant emission peak. One can see that with the increase of the width of the core, the photoluminescence intensity is decreased. This phenomenon can be explained by two reasons: (1) Because the sheaths of the ribbon-shaped coaxial conductive nanocables are transparent, the exciting and emitting light are absorbed by the dark-colored PANI and Fe_3O_4 NPs in the cores. From the UV-vis absorption spectra of PANI and Fe_3O_4 NPs illustrated in the right figure in **Figure 8**, it can be seen that both the PANI and Fe_3O_4 NPs can absorb visible light (400-700 nm) and much more easily absorb the ultraviolet light (< 400 nm). Thus, the exciting light and emitting light are absorbed by the $Fe_3O_4/PANI/PMMA$ core and the intensities are decreased. Furthermore, the light absorption would become stronger with increasing the width of the core. (2) As seen in the **Figure 6**, the ribbon-shaped nanocables fabricated using different inner stainless-steel needles almost have the same width, so that the content of the photoluminescent $Tb(BA)_3phen$ complex in single ribbon-shaped coaxial conductive nanocable is decreased with the increase of the width of the core. **Figure 9** illustrates the photoluminescence process of the ribbon-shaped coaxial conductive nanocables with different width of cores. The exciting light and emitting light which are not affected by the cores contribute most to the photoluminescence intensity ("strong" section), whereas the exciting light and emitting light which are absorbed by the cores contribute only a little ("weak" section). The overall result is that the photoluminescence intensity is reduced with the reduction of "strong" section.
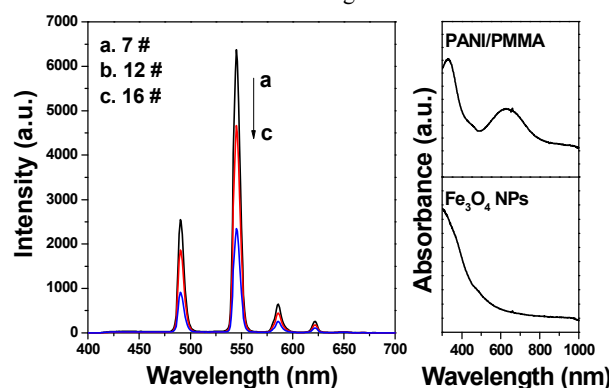
Fig. 8 Photoluminescence emission spectra (excited by 333-nm ultraviolet light) of the ribbon-shaped coaxial conductive nanocables arrays fabricated using 7 # (a), 12 # (b) and 16 # (c) inner stainless-steel needles (left figure) and UV-vis absorption spectra of PANI/PMMA and Fe_3O_4 NPs (right figure)

Fig. 9 Photoluminescence schematic diagrams of ribbon-shaped coaxial conductive nanocables fabricated using 7 # (a), 12 # (b) and 16 # (c) inner stainless-steel needles

Magnetic properties

The typical hysteresis loops for ribbon-shaped coaxial conductive nanocables arrays fabricated using different inner stainless-steel needles are shown in **Figure 10**. It is well known that the saturation magnetization of a magnetic composite material

depends on the mass percentage of the magnetic substance in the magnetic composite material.[21-23] The saturation magnetization of the ribbon-shaped coaxial conductive nanocables array is increased with the increase of width of the cores of the ribbon-shaped coaxial conductive nanocables in the array, indicating that the magnetic performance of the nanocables array can be tuned by adding various amount of Fe_3O_4 NPs. The magnetic properties

of the ribbon-shaped coaxial conductive nanocables arrays indicate that the ribbon-shaped coaxial conductive nanocables arrays can be easily manipulated by controlling the applied magnetic field.
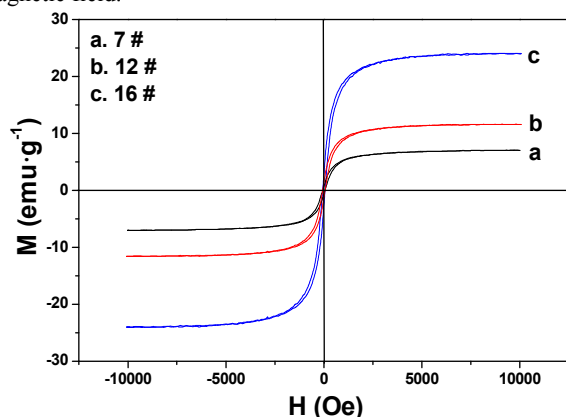
Fig. 10 Hysteresis loops for ribbon-shaped coaxial conductive nanocables arrays fabricated using 7 # (a), 12 # (b) and 16 # (c) inner stainless-steel needles

Conclusions

In summary, novel flexible [Fe$_3$O$_4$/PANI/PMMA]@[Tb(BA)$_3$phen/PMMA] ribbon-shaped coaxial conductive nanocables arrays with electric conductivity, magnetism and photoluminescence have been successfully fabricated by electrospinning using specially designed coaxial spinneret. The arrays are composed of ribbon-shaped coaxial conductive nanocables arranged in the same direction. Each ribbon-shaped coaxial conductive nanocable in the array consists of a Fe$_3$O$_4$/PANI/PMMA conductive-magnetic bifunctional core and a Tb(BA)$_3$phen/PMMA insulating photoluminescent sheath, so that each ribbon-shaped coaxial conductive nanocable is insulated with each other in the array. The width of every single ribbon-shaped coaxial conductive nanocable is ca. 10 μm and the thickness is ca. 879 nm. The width of the core of a ribbon-shaped coaxial conductive nanocable can be easily tuned just by changing the inner stainless-steel needle in the coaxial spinneret. The electric conductance of each single ribbon-shaped coaxial conductive nanocable can be calculated by given formula and available experimental data. The ribbon-shaped coaxial conductive nanocables arrays can emit green light under ultraviolet light and have response in the magnetic field. The conductivity, magnetism and photoluminescence of the ribbon-shaped coaxial conductive nanocables arrays can be tunable by adjusting the contents of PANI and Fe$_3$O$_4$ NPs and rare earth complexes, or by varying the width of the cores of the every ribbon-shaped coaxial nanocable in the array. The ribbon-shaped coaxial conductive nanocables arrays resolve many deficiencies of the existing nanocables, such as high brittleness, short length, poor visibility and controllability, to accord with practical applications.

Acknowledgments

Notes and references

Key Laboratory of Applied Chemistry and Nanotechnology at Universities of Jilin Province, Changchun University of Science and Technology, Changchun 130022. Fax: 86 0431 85383815; Tel: 86 0431 85582574; E-mail: dongxiangting888@163.com

1 A. Zahoor, Q. Teng, H. Wang, M. A. Choudhry and X. Li, *Met. Mater. Int.,* 2011, **17**, 417.
2 M Miyauchi, J. Miao, T. J. Simmons, J. W. Lee, T. V. Doherty, J. S. Dordick and R. J. Linhardt, *Biomacromolecules,* 2010, **11**, 2440.
3 G. She, X. Zhang, W. Shi, Y. Cai, N. Wan, P. Liu and D. Chen, *Cryst. Growth Des.,* 2008, **8**, 1789.
4 S. Kumar, V. Kundu, A. Vohra and S. K. Chakarvarti, *J. Mater. Sci.: Mater. Electron.,* 2011, **22**, 995.
5 T. H. Han, W. J. Lee, D. H. Lee, J. E. Kim, E. Y. Choi and S. O. Kim, *Adv. Mater.,* 2010, **22**, 2060.
6 Z. Li, H. Huang and C. Wang, *Macromol. Rapid Comm.,* 2006, **27**, 152.
7 S. Guo, J. Li, W. Ren, D. Wen, S. Dong and E. Wang, *Chem. Mater.,* 2009, **21**, 2247.
8 Z. Zhou, J. Zhao, Z. Chen, X. Gao, J. Lu, P. R. Schleyer and C. K. Yang, *J. Phys. Chem. B,* 2006, **110**, 2529.
9 J. Song, M. Chen, M. B. Olesen, C. Wang, R. Havelund, Q. Li, E. Xie, R. Yang, P. Bøggild, C. Wang, F. Besenbacher and M. Dong, *Nanoscale,* 2011, **3**, 4966.
10 J. Jang, B. Lim, J. Lee and T. Hyeon, *Chem. Commun.,* 2001, **1**, 83.
11 W. Sambaer, M. Zatloukal and D. Kimmer, *Chem. Eng. Sci.,* 2011, **66**, 613.
12 J. M. Corres, Y. R. Garcia, F. J. Arregui and I. R. Matias, *IEEE Sens. J.,* 2011, **11**, 2383.
13 A. Townsend-Nicholson and S. N. Jayasinghe, *Biomacromolecules,* 2006, **7**, 3364.
14 S. L. Chen, H. Q. Hou, F. Harnisch, S. A. Patil, A. A. Carmona-Martinez, S. Agarwal, Y. Y. Zhang, S. Sinha-Ray, A. L. Yarin, A. Greiner and U. Schröder, *Energy Environ. Sci.,* 2011, **4**, 1417.
15 Z. Hou, X. Li, C. Li, Y. Dai, P. Ma, X. Zhang, X. Kang, Z. Cheng and J. Lin, *Langmuir,* 2013, **29**, 9473.
16 M. Zhang, C. Shao, J. Mu, X. Huang, Z. Zhang, Z. Guo, P. Zhang and Y. Liu, *J. Mater. Chem.,* 2012, **22**, 577.
17 Z. Zhang, C. Shao, X. Li, Y. Sun, M. Zhang, J. Mu, P. Zhang, Z. Guo and Y. Liu, *Nanoscale,* 2013, **5**, 606.
18 D. Li, Y. Wang and Y. Xia, *Nano Letters,* 2003, **3**, 1167.
19 M. J. Laudenslager and W. M. Sigmund, *J. Nanopart. Res.,* 2013, **15**, 1487.
20 L. Persano, C. Dagdeviren, Y. Su, Y. Zhang, S. Girardo, D. Pisignano, Y. Huang and J. A. Rogers, *Nat. Commun.,* 2013, **4**, 1633.
21 Q. Ma, W. Yu, X. Dong, J. Wang, G. Liu and J. Xu, *J. Nanopart. Res.,* 2012, **14**, 1203.
22 Q. Ma, J. Wang, X. Dong, W. Yu, G. Liu and J. Xu, *J. Mater. Chem.,* 2012, **22**, 14438.
23 Q. Ma, W. Yu, X. Dong, J. Wang, G. Liu and J. Xu, *Opt. Mater.,* 2013, **35**, 526.
24 G. Gai, L. Wang, X. Dong, C. Zheng, W. Yu, J. Wang and X. Xiao, *J. Nanopart. Res.,* 2013, **15**, 1539.
25 N. Lv, Q. Ma, X. Dong, J. Wang, W. Yu and G. Liu, *Chem. Eng. J.,* 2014, **243**, 500.
26 Q. Ma, W. Yu, X. Dong, J. Wang and G. Liu, *Nanoscale,* 2014, **6**, 2945.
27 Q. Ma, J. Wang, X. Dong, W. Yu and G. Liu, *ChemPlusChem,* 2014, **79**, 290.
28 C. Song and X. Dong, *J. Optoelectron. Adv. Mater.,* 2012, **6**, 319.
29 G. H. Lee, J. C. Song and K. B. Yoon, *Macromol. Res.,* 2010, **18**, 571.

Graphical Abstract
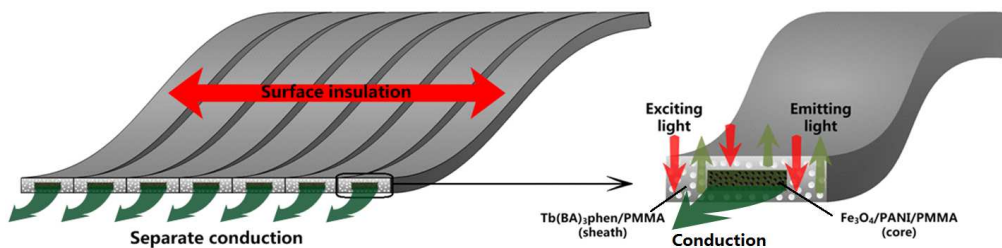
A new type of flexible ribbon-shaped coaxial conductive nanocables array possessing conductivity, magnetism and photoluminescence can be achieved by one-pot electrospinning using a specially designed coaxial spinneret. All the ribbon-shaped coaxial nanocables are insulated with each other and arranged in array alignment. The ribbon-shaped coaxial nanocables array is simultaneously endowed with magnetic and photoluminescent characteristics for improving controllability and visibility.